Electronic Supplementary Material (ESI) for Environmental Science: Nano.

Supporting Information

Scalable and Eco-Friendly Fabrication of Anti-Oil-Fouling Solar Interfacial Evaporator for Efficient Water Purification

Jiaying Wang[1a], Yuxia Xu[1a], Yang Guo[a], Juan Wang*[a]

[a] MOE Key Laboratory of Environmental Remediation and Ecosystem Health, College of Environment and Resources Science, Zhejiang University, Hangzhou 310058, China

*Corresponding author:

Juan Wang, 866 Yuhangtang Road, Hangzhou 310027, P.R. China. E-mail address: wjuan@zju.edu.cn.

[1] Jiaying Wang and Yuxia Xu contributed equally to this study.

Table of Content

Note S1. Calculation of the phase-change enthalpy

The phase-change enthalpy of water consists of two parts: sensible heat and latent heat. The total enthalpy is calculated by the following Eq. 1 [1]:

$$h_{lv} = C\Delta T + h_{lat} \tag{1}$$

where C is the specific heat capacity of water (1.16×10^{-3} kW h kg^{-1} K^{-1}), ΔT is the temperature difference between the water evaporation surface (T_{evap}, K) and source water (~297 K).

The latent heat of liquid-vapor phase change (h_{lat}, kw h kg^{-1}) is calculated given by an empirical formula (Eq. 2)[2]:

$$h_{lat} = 0.5329\left(\frac{T_{evap}}{T_{evap} - 33.91}\right)^2 \tag{2}$$

where T_{evap} is the surface temperature of the evaporation surface (T_{evap}, K).

Note S2. Calculation of the solar-to-vapor conversion efficiency

The water evaporation rates under one sun illumination are calculated by Eq. 3 below:

$$E = \Delta m/(A_{proj}\Delta t) \tag{3}$$

where Δm is the mass loss recorded by a laboratory balance (kg) in the time period Δt (h) at steady state, and A_{proj} is the projected area that represents the evaporation area (m^2).

The solar-to-vapor conversion efficiencies under one sun can be calculated by the following formula:

$$\eta = \frac{(E_{light} - E_{dark})h_{lv}}{q_{solar}} \tag{4}$$

where E_{light} is the evaporation rate under one sun illumination, E_{dark} is the evaporation rate under dark condition, h_{lv} is the water phase-change enthalpy from liquid to vapor (kW h kg^{-1}), q_{solar} is the solar irradiation intensity (1 kW m^{-2}).

Note S3. Calculation of solar absorption

The solar absorption at the wavelength λ is given by:

$$A(\lambda) = 1 - R(\lambda) - T(\lambda)$$

where $R(\lambda)$ and $T(\lambda)$ are the reflection and transmission of a sample at the wavelength λ, respectively.

And the solar absorption (A) weighted by AM 1.5 G spectrum is given by[3]:

$$A = \frac{\int_{0.3\ \mu m}^{2.5\ \mu m} I_{solar}(\lambda)A(\lambda)d(\lambda)}{\int_{0.3\ \mu m}^{2.5\ \mu m} I_{solar}(\lambda)d(\lambda)}$$

where $I_{solar}(\lambda)$ and $A(\lambda)$ are the solar spectral irradiance and absorption of a sample at the wavelength λ, respectively.

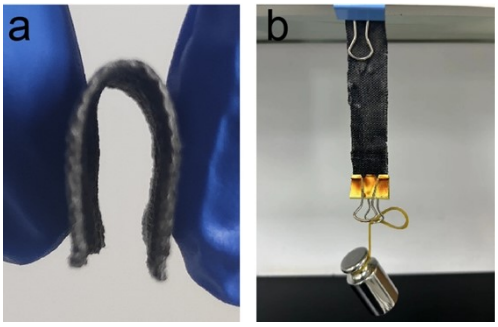

Figure S1. The digital photographs of the CCCF during the (a) bending and (b) stretching test. The obtained fabric presents a flexible property.

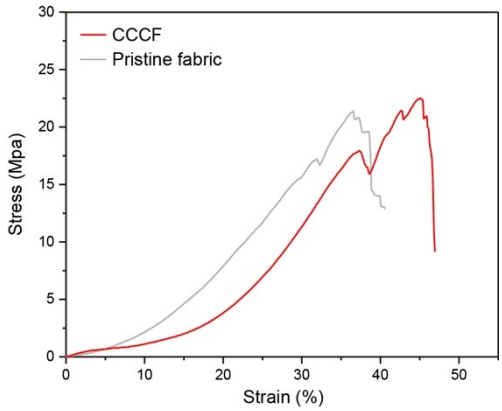

Figure S2. Stress-strain curves of CCCF and pristine fabric.

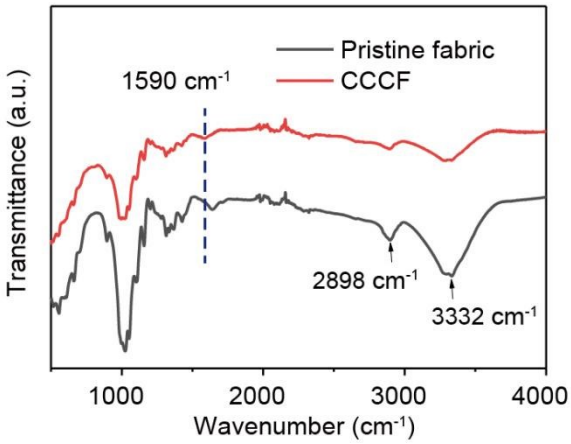

Figure S3. FTIR spectra of pristine fabric and CCCF.

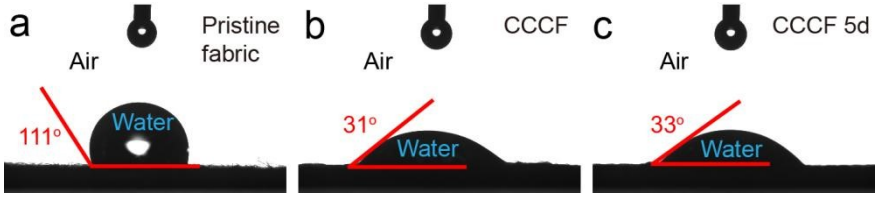

Figure S4. WCA of (a) pristine fabric, (b) synthesized CCCF and (c) synthesized CCCF leaving after five days.

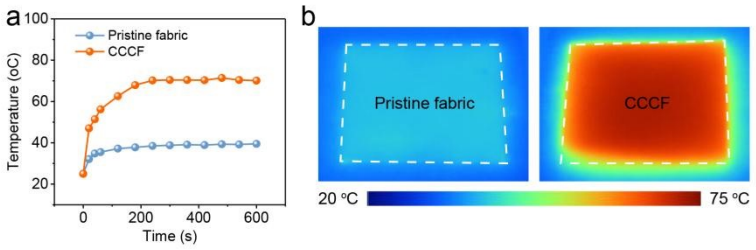

Figure S5. (a) Surface temperature change of the pristine fabric and CCCF in the dry state under one sun. (b) IR images of the pristine fabric and CCCF in the dry state under one sun when the temperature is stable.

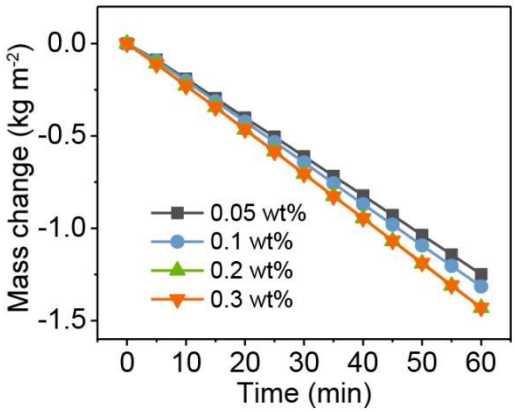

Figure S6. Mass change of the CCCFs obtained with different initial carbon black concentrations under one sun during the evaporation test. Various CCCFs were synthesized with different CB concentrations including 0.05wt %, 0.1wt %, 0.2wt % and 0.3wt %. The calculated corresponding water evaporation rates were 1.27, 1.34, 1.44 and 1.46 kg m^{-2} h^{-1}, respectively. Therefore, the fabrics based on 0.2wt % CB concentration were adopted for the experiment.

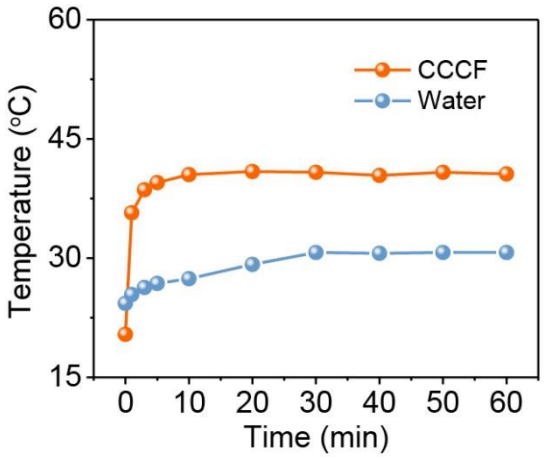

Figure S7. Temperature change over time of the evaporating water and CCCF under one sun.

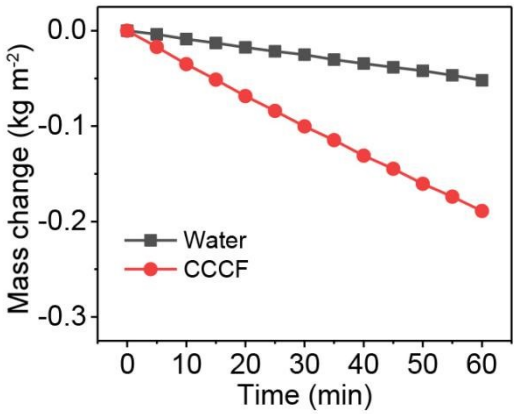

Figure S8. Mass change of the evaporating water and CCCF under dark condition.

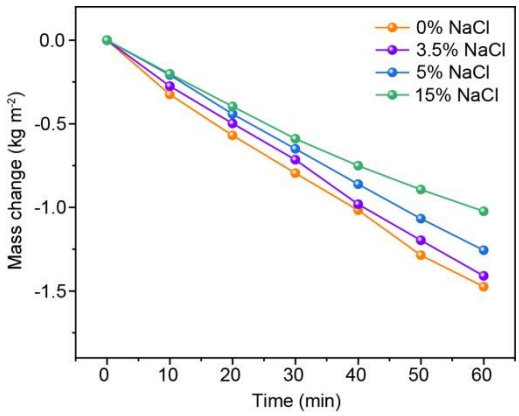

Figure S9. Mass change of the CCCF in different salt solutions under one sun.

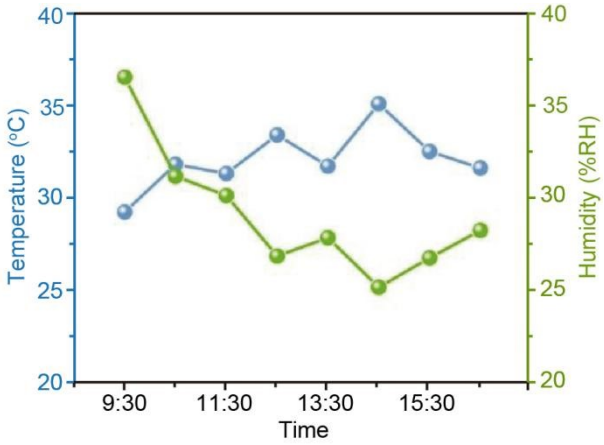

Figure S10. Temperature and relative humidity over 9:30-16:30 during the outdoor experiment.

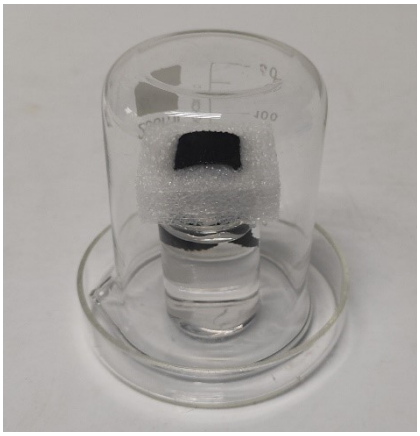

Figure S11. Photograph of the laboratory condensation set. A big beaker placed on a petri dish was adopted to collect the vapor generated from the CCCF-based evaporator.

Table S1. Performance comparison of the evaporators based on the underwater superoleophobic and photothermal materials

Name	Evaporation rate ($kg\ m^{-2}\ h^{-1}$)	Stability test condition	Notes
[4]Wood-TA-Fe^{3+}	1.85	acid solution (pH=2, 24 h), alkaline solution (pH = 12, 24 h), seawater flushing (3000 r/min, 100 h), cyclic freeze-thaw (100 times), ultrasonication (2 h)	test results of light absorption and underwater oil contact angle after treatment are not provided
[5]Wood-PVA-CNT	1.35	acid solution (pH=1, 24 h), alkaline solution (pH = 13, 24 h)	photothermal layer is not tested
[6]Cotton-	1.54	acid solution (pH=3, 48 h),	/

PPy/GA/APTES (PGCF)		alkaline solution (pH = 11, 48 h), saline soaking (48 h), ultrasonication (30 min)	
This work	1.44	acid solution (pH=1, 48 h), alkaline solution (pH = 11, 48 h), saline soaking (48 h), ultrasonication (30 min), heating (3h)	/

Supplementary references

1 X. Li, R. Lin, G. Ni, N. Xu, X. Hu, B. Zhu, G. Lv, J. Li, S. Zhu and J. Zhu, *Natl. Sci. Rev*., 2017, **5**, 70-77.

2 B. Hendersonsellers, *Q. J. R. Meteorol. Soc.,* 1984, **110**, 1186-1190.

3 L. Zhou, Y. Tan, J. Wang, W. Xu, Y. Yuan, W. Cai, S. Zhu and J. Zhu, *Nat. Photon.,* 2016, **10**, 393-398.

4 F. He, M. Han, J. Zhang, Z. Wang, X. Wu, Y. Zhou, L. Jiang, S. Peng and Y. Li, *Nano Energy* 2020, **71**, 104650.

5 Z. Wang, P. Guo, L. Heng ans L. Jiang, *Matter* 2021, **4**, 1274-1286.

6 Y. Xu, T. Xu, Y. Guo, W. P. Liu, J. Wang, *Sep. Purif. Technol*., 2023, **312**, 123289.